Robotic Metamaterials: A Modular System for Hands-On Configuration of Ad-Hoc Dynamic Applications

Zhitong Cui
zhitongc@andrew.cmu.edu
Human-Computer Interaction
Institute, School of Computer Science,
Carnegie Mellon University
USA

Shuhong Wang
shuhongw@andrew.cmu.edu
Human-Computer Interaction
Institute, School of Computer Science,
Carnegie Mellon University
USA

Violet Yinuo Han
yinuoh@andrew.cmu.edu
Human-Computer Interaction
Institute, School of Computer Science,
Carnegie Mellon University
USA

Tucker Rae-Grant
traegran@andrew.cmu.edu
Human-Computer Interaction
Institute, School of Computer Science,
Carnegie Mellon University
USA

Willa Yunqi Yang
yunqiy@andrew.cmu.edu
Human-Computer Interaction
Institute, School of Computer Science,
Carnegie Mellon University
USA

Alan Zhu
aczhu@andrew.cmu.edu
Human-Computer Interaction
Institute, School of Computer Science,
Carnegie Mellon University
USA

Scott E. Hudson
hudson@andrew.cmu.edu
Human-Computer Interaction
Institute, School of Computer Science,
Carnegie Mellon University
USA

Alexandra Ion
aion@andrew.cmu.edu
Human-Computer Interaction
Institute, School of Computer Science,
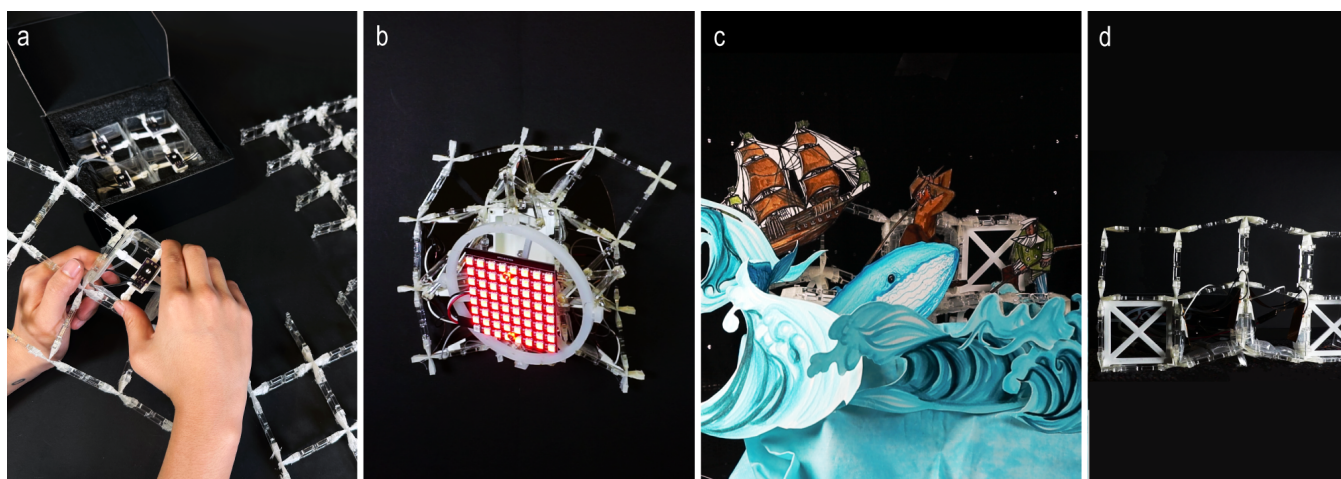Carnegie Mellon University
USA

Figure 1: (a) Our initially passive metamaterial can be configured with active elements to implement robotic functions such as (b) a robotic wall material, e. g., programmable spotlights, (c) custom mechanisms such as a robotic play, or (d) a crawling robot.

ABSTRACT

We propose augmenting initially passive structures built from simple repeated cells, with novel active units to enable dynamic, shape-changing, and robotic applications. Inspired by metamaterials that can employ mechanisms, we build a framework that allows users to configure cells of this passive structure to allow it to perform complex tasks. A key benefit is that our structures can be repeatedly (re)configured by users inserting our configuration units to turn the passive material into, e.g., locomotion robots, integrated motion platforms, or interactive interfaces, as we demonstrate in this paper.

To this end, we present a mechanical system consisting of a flexible, passive, shearing lattice structure, as well as rigid and active unit cells to be inserted into the lattice for configuration. The active unit is a closed-loop pneumatically controlled shearing cell to dynamically actuate the macroscopic movement of the structure. The passive rigid cells redirect the forces to create complex motion with a reduced number of active cells. Since the placement of the rigid and active units is challenging, we offer a computational design tool. The tool optimizes the cell placement to match the macroscopic, user-defined target motions and generates the control code for the active cells.

CCS CONCEPTS

• **Human-centered computing → Interactive systems and tools**.

KEYWORDS

metamaterials, reconfigure, fabrication, 3D printing, elasticity, programmable matter, HCI

1 INTRODUCTION

Advancements in digital fabrication technology can democratize making. To enable users to go beyond static shapes [20, 25], HCI researchers have investigated systems enabling the fabrication of functional and dynamic objects ranging from mechanical objects [10, 27], compliant mechanisms[18, 40], shape-changing interfaces [23, 41], soft robotics [9, 37], to programmable materials [11, 13, 14]. We observe a trend from static shapes towards dynamic and compliant mechanical objects.

One example of such programmable materials is so-called metamaterials [1], which are artificial microstructures that define the macroscopic material properties. Going beyond designing material properties, researchers started to view metamaterials as machines. Such metamaterial mechanisms are passive materials that can employ mechanical [11] or computational [14] functions and can typically be fabricated in one piece and without the need for assembly. However, the mechanisms implemented by these structures are passive and cannot be modified after fabrication, i. e., if users don't need their mechanism anymore, they have no opportunity to upgrade it and might need to dispose it.

In this paper, we propose an integrated modular approach to allow users to create dynamic, interactive metamaterials that can provide robotic functions, and which can be reconfigured later to change or replace their function. Users can configure an initially passive lattice by inserting actuation units that we call *active cells*. Along with passive rigid cells, they provide a modular reusable platform for users to design robotic and shape-changing applications in a hands-on fashion. Our paper presents an enabling technology to explore novel interactions with robotic materials, which arise from

possibilities for users to size, shape, integrate with existing objects, repeatedly configure, and control their robotic material in-situ and hands-on to perform different tasks.

1.1 Elements of our Robotic Metamaterial

To explore our modular robotic platform, we design it with three simple building blocks and present prototypical implementations in this paper. The elements that our robotic material consists of are (1) passive shearing cells, (2) passive rigid cells, and (3) active shearing cells, as we illustrate in Figure 2. The basic cell system building on careful placement of shearing and rigid cells is inspired by previous work on Metamaterial Mechanisms [11, 13].
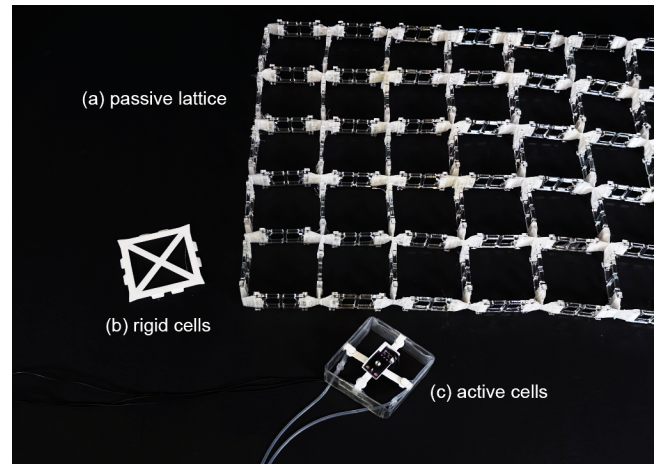

Figure 2: Our robotic metamaterial consists of (a) a passive lattice of shearing cells, (b) passive rigid cells, and (c) a novel active cell that is (d) pneumatically actuated to enable configurable robotic function.

Figure 2a shows the generic sheet of passive shearing cells. Each of these cells implements a four-bar linkage, i.e., a 1 degree of freedom mechanism that enables a controlled directional movement. Users can configure the robotic movement by inserting rigid cells (see Figure 2b), which propagate forces through the material and in concert with the shearing cells implement mechanisms.

We extend the capabilities of such materials by introducing an *active cell* to actuate the material, which we show in Figure 2c. Like the rigid cells, this active cell can also be placed into the passive shear lattice such that users can configure their metamaterial repeatedly to implement desired robotic functions. The active cell is pneumatically actuated and contains a rotary angle sensor for position feedback.

1.2 Walkthrough

In the following, we showcase how users configure our metamaterial to implement custom mechanisms. We envision our material being useful in, e. g., classroom scenarios to increase student engagement. Consider the example of a second-grade teacher planning to teach classic American literature to their students; in this case the well-known story of Moby Dick. To make this lecture engaging for

the young kids, the teacher decides to prepare a robotic theatrical version of the story, as illustrated in Figure 3.
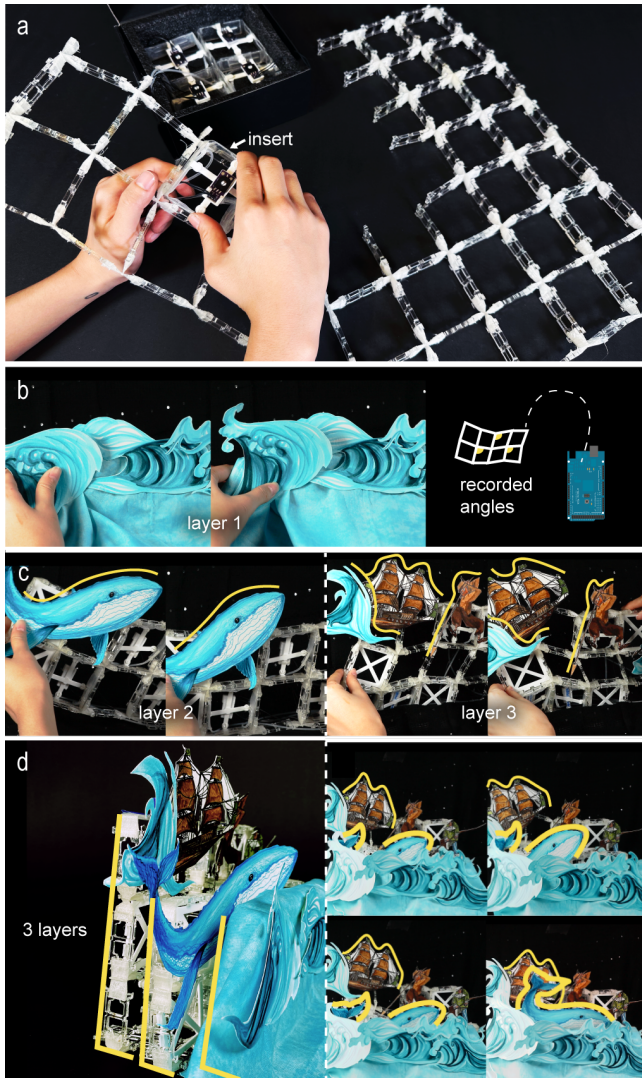

Figure 3: (a) The user tears off a smaller piece of the passive lattice they received, and inserts active cells into the lattice. (b) The user demonstrates motions to one layer of the Robotic Metamaterial, this motion is recorded for the material to playback on its own. (c) The user decides to add multiple layers, they demonstrate motions for two additional layers. (d) Three layers of Robotic Metamaterials play the recorded motions designed by the user, forming a story scene.

(a) Sizing the material. The teacher gets the passive shearing lattice that is part of our Robotic Metamaterial system. This lattice serves as the base structure, is generic, and can be used like a stock material. They tear off a smaller piece that fits into the puppet-sized stage they plan to use. Next, they insert and connect active cells into the passive lattice to prepare the movements.

(b) Designing the target motion. The teacher demonstrates the motion of waves in water, which they want the lattice to perform in the theater play. To do so, they deform the material manually. Since they have inserted active cells with sensing capabilities, the cells record the motion by tracking the angles over time. The user is playing the demonstrated motion back to see its effect.

(c-d) Adding more layers. The teacher decides to add multiple layers of our Robotic Metamaterial to highlight more scenes and give the theatrical demonstration of the story more complexity. They get two more pieces of the passive lattice, insert active cells, and demonstrate the desired movement for each layer: the second layer will animate the whale in the ocean, while the third layer integrates the ship and Captain Ahab. After recording the movement, the teacher uses the robotic metamaterial with attached cutouts as a part of their lesson. After the class, they may reconfigure their Robotic Metamaterials to support other stories, by changing the size of the lattice, or the number or placement of cells.

More design capabilities. In the remainder of this paper, we will showcase how our Robotic Metamaterial can be further customized and applied to a variety of applications, including integrated into furniture, walls, or performing robotic functions, as illustrated in Figure 1. In addition to the hands-on demonstration of movement to the materials, we also implement a computational design tool that supports users in creating complex paths. We describe in Section 5 how our software optimizes the cell placement for rigid and active cells and computes the angles to be actuated given a desired motion path.

1.3 Contributions, Benefits, and Limitations

The main *contribution* of this work is the concept of dynamic metamaterials to perform robotic movements based on metamaterial mechanisms. To investigate the potential impact of such robotic materials, we make the following specific contributions.

(1) We develop prototypes of modular *active unit cells* to dynamically actuate the macroscopic movement of a larger structure. Our structures can be repeatedly (re)configured by users inserting our configuration units to implement their specific applications, making our design *reusable*.

(2) We offer *hands-on manipulation* to users. They can 'program' the material by deforming it manually to demonstrate its desired motion. Our material therefore acts as input and output devices.

(3) Complementary, we also contribute a computational *design tool* that optimizes the cell placement to match more complex, macroscopic, user-defined target motions and generates the control code for the active cells.

(4) We also contribute an initial overview of example *applications* to investigate the utility of such Robotic Metamaterials in the future.

Benefits. The key benefit of our system is that it is *modular*, *reusable*, and *programmable*, which allows users to opportunistically create robotic materials that can be repeatedly configured for *multiple functions*. The programmability and reconfigurability of our material empowers users to create robots in-situ. Users can reconfigure the lattice into different sizes or layers to adapt to their

specific needs. Our resulting robotic materials are soft and safe to interact with. While a number of other shape-changing systems may show similar use cases, the benefit of our system is that users can flexibly create all demonstrated applications with simple building blocks. Additionally, from a research perspective, our work bridges between shape-changing interfaces, soft robotics, and mechanical metamaterial, encouraging us to think of materials and robotics on a spectrum and explore the resulting interaction and integration possibilities.

Limitations. However, the resulting robotic systems are also subject to limitations. Since our cells rely on compliant deformation, they suffer from the same limitations as compliant mechanisms: as the lattice size increases, its resistance increases as well, meaning that more active cells are necessary to drive the desired motion. Our robotic materials also can't produce any continuous rotation, like axles in traditional mechanisms. Additionally, we only explore 2D robotic metamaterials and 2.5D multi-layer metamaterials. A practical limitation of our research prototypes is that they use inexpensive hardware and are handmade, rather than professionally manufactured, which can lead to inconsistencies in their behavior. Consequently, the size of our unit cells is larger yet demonstrates the working principle and interaction.

2 RELATED WORK

Our work builds on previous work in the areas of shape-changing interfaces, soft robotics, and mechanical metamaterials.

2.1 Shape-Changing Interfaces

Shape-changing interfaces with pneumatic actuation have been explored in the HCI field. The project PneUI created shape-changing interfaces through pneumatically actuated soft composite materials [41]. Project Sticky Actuators proposed planar soft actuators that can be pneumatically controlled and actuate everyday passive objects [21]. Researchers have also started to transform everyday materials into different shapes and actuation mechanisms. Ou et al. created bending mechanisms that transform inflatables made of various materials into different shapes [23]. Choi and Ishii explored heat-seal patterning that transforms everyday material into DIY inflatables [3]. These techniques, however, offer limited interactivity as it is hard to configure those materials after fabrication. Different from prior work, our shape-changing material can be repeatedly configured after fabrication by end users. Our work provides a modular platform to allow users to create interactive materials.

2.2 Soft Robotics

The domain of soft robotics creates robots from soft components. This is a broad area of work, however, as exemplars, researchers have created pliant structures through programmable composites [17], mechanical structures [42], mechanisms [36], etc. to build soft actuators [19], locomotion robots [8, 34], etc. Pneumatic actuation is common in soft robotics as it can control complex motion with simple actuation [4, 31]. Our proposed robotic material consists of rigid plates connected through flexible joints, making the whole material sheet compliant and flexible. In contrast to actuating the entire material sheets globally, we focus on actuating local areas of the material to trigger the desired global deformation.

2.3 Mechanical Metamaterials

Mechanical metamaterials offer advanced material properties due to their internal mechanical structures. For example, varied internal structures that are 3D printed or laser cut can offer varied elasticity to allow bending and rotation of desired parts [29, 32]. A metamaterial sheet with auxetic structures allows two-dimensional expansion upon a one-dimensional stretch [15, 28] and both planar and spatial transformations [22]. Recently, metamaterials have started to be understood as devices. Ion et al. implemented mechanisms from metamaterials with repeated shear structures [11]. Shaw et al. made compliant mechanisms from rolling-contact architected structures [30]. Mechanisms can trigger texture change such as the texture on a bike handle [12]. Researchers have also started to integrate circuits into the material [7] and allow in-material sensing capability [5]. Going beyond passive materials that rely on external forces, researchers have started to dynamically actuate materials. Yang et al. implemented an actuated soft buckling mechanism that can switch between two states under actuation [39]. Overvelde et al. designed a 3D metamaterial that can have multiple degrees of freedom [24]. Yang et al. 4D printed a lattice structure that changes shape under temperature change [38]. Besides the global shape reconfiguration, researchers have also investigated locally reprogrammable materials to offer more material configuration potentials. Chen et al. implemented metamaterials that can be locally reconfigured using a machine [2]. These actuated materials, however, offer limited capacity for shape change and complexity of movements. The robotic metamaterials we propose in this project offer high customizability and complexity of shape-changing while being easy to reconfigure.

3 ACTIVE CELL IMPLEMENTATION

A key feature of the work described here is that a range of different functional motions can be implemented using only a very small number of different generic and reusable component types, i. e., a uniform flexible lattice in a grid structure, a passive rigid component that can be inserted in a grid cell, and an active actuation and sensing cell. Each of these component types is generic and reusable. This means that a lattice configured for one or more motions can repeatedly be reconfigured for a different purpose. In the following, we describe the core component of our robotic metamaterial: our active cell. This component is a modular actuator that can be inserted in any cell in the flexible lattice. It employs pneumatic actuation and angle sensing for closed-loop control.

3.1 Pneumatic Actuation

Our active cell employs pneumatic actuation. The working principle is shown in Figure 4 and inspired by prior work [11, 24]. The structure of our active cell is a shear cell, i.e., it can change its angle while the opposing members remain parallel. It is a mechanism with 1 degree of freedom. The air pockets for our pneumatic actuation are attached to adjacent corners. When a pocket inflates, the adjacent members are flattened out. To achieve this in both directions, we use two air pockets working in opposition within each shear cell.

We opted for pneumatic actuation as it yields compliant actuation, making our material conformable and robust against potential
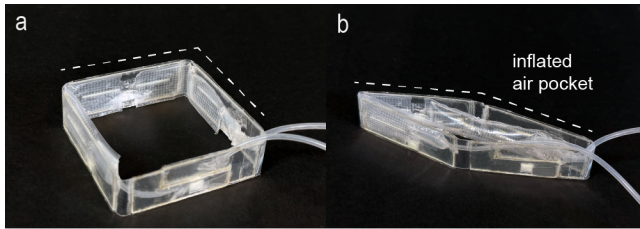
Figure 4: (a) The active cell is actuated by air pockets located in its corners, top left and right in this example. (b) We show how as the air pocket inflates, the angle increases and the adjacent members flatten.

Figure 6: Versions of our active cell featured (a) capacitive sensing, (b) improved actuation strength but difficult control, and (c) the rotary sensor but without being easy to insert. We use different active cells throughout our demonstrations, as they were developed at different stages of this work.

impact. Furthermore, we favored it for its potential for miniaturization. While an air supply (e.g., a compressor) is needed, it does not have to be built into the material but can be supplied from a distance.

3.2 Angle Sensing

We integrate a rotary sensor into each active cell using a scissor mechanism. As shown in Figure 5, the sensor (a CJMCU-130 compact potentiometer) measures the angle between the scissor legs, and hence the shear angle of the cell. We attach these scissor legs to the underlying cell's four walls via snap-fit pins. The upper scissor leg contains a sensor holder with a slot at the sensor's rotating element. The lower scissor leg contains a vertical snap-fit bar at the same location which meshes with a hole in the sensor's rotating element to form a pin joint to mechanically drive the sensor.
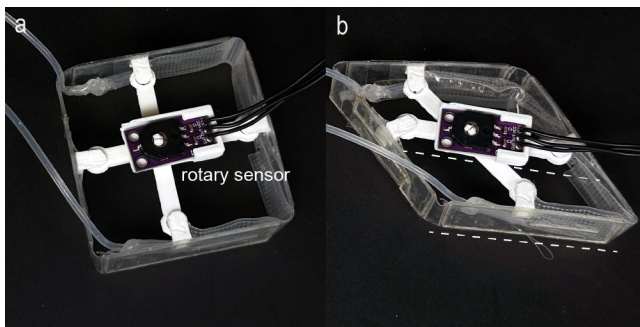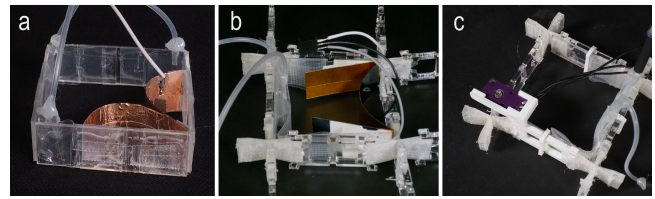

Figure 5: (a) We integrate a rotary sensor into the cell geometry via a scissor mechanism, (b) ensuring that the sensor stays parallel with the cell's walls during shearing motions.

This sensor mechanism allows us to measure the shear angle of the cell accurately and thus provides the basis for closed-loop control of the active cell. We developed multiple versions of our active cell, shown in Figure 6, which used capacitive sensing (a), improved actuation strength (b), but could not be inserted easily into the lattice (b-c).

3.3 Closed-loop Control

We use the sensor data to implement closed-loop control for our pneumatic actuation. Each active cell is controlled by 4 valves,

i.e., two valves per actuated corner. We use simple 2-way (on-off) solenoid valves in our prototypes that can operate at 0 psi[1]. For each pneumatic bag, one valve controls the connection to the air compressor ("supply") and one valve controls the connection to the environment ("exhaust"). By alternately opening and closing the supply and exhaust valves for a short duration, we can inflate or deflate the bags in metered increments. To drive the active cell to achieve a certain angle, our actuation principle is to inflate one airbag while deflating the other, such that the opposing airbag doesn't hinder cell movement. To deflate the opposing airbag, we open its exhaust valve to let the inflating airbag push out the air of the deflating bag. Our control loop manages the amount of air to inflate the bag to reach the desired angle. When there are multiple active cells to be actuated, our control loop actuates them sequentially via the Arduino Timer with precise duration control. We also implemented a PID (Proportional Integral Derivative) method based on the sensor data which adjusts the actuation time for each airbag. The parameters for the PID controller are tuned to actuate the cells to quickly reach the target angle without significant overshooting problems. A moving average filter function is used to smooth the sensor readings.

To drive the active cells, we connect the driver modules to the global power source (12V DC) and air supply (Master Airbrush Cool Runner II, 57psi compressor). An Arduino Mega board is used to drive all the relays and valves based on the sensor data. In our current prototypes, we use approx. 30 psi from the air supply to drive the active cells effectively. We illustrate our auxiliary driving setup for a single active cell in Figure 7.

3.4 Fabrication of our Research Prototypes

Given that this is a modular system, we envision that the components could eventually be mass-manufactured and end-users would buy them as part of a construction kit. Users would treat the passive lattice as a reusable stock material (as they might a sheet of acrylic), and insert our passive rigid cells, as well as our active actuation and sensing elements from the kit. We do not suggest that users would build these cells. However, to foster replicability of our work, we describe the fabrication process of our prototypes in the following, and supplement a step-by-step tutorial and 3D model files.
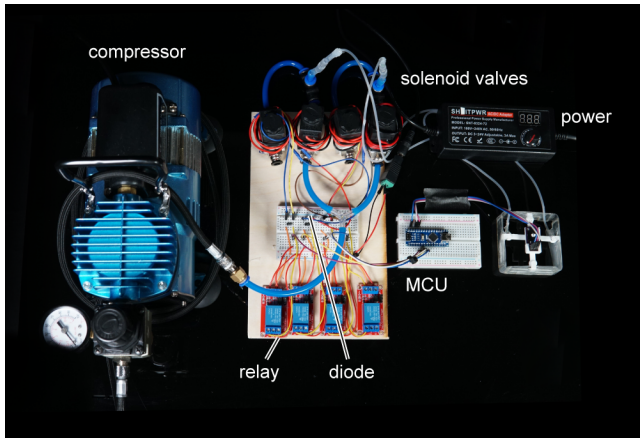
---

[1]pound-force per square inch

Figure 7: The entire circuit includes valves and relays for each active cell, and shared power supply, compressor for air supply, and a microcontroller.

3.4.1 Active cell fabrication. Below we describe the fabrication process of the key component of our work: the active cell module, as illustrated in Figure 8.

Each of a cell's four walls is a 15×50 mm rectangle of laser cut 1 mm thick acrylic, with engravings (highlighted in yellow in Figure 8a) informing precise attachments of other cell components. After cutting the cell walls, we leave them in the laser cutter and laminate a layer of tape to keep the cell walls' positions intact. Then, we take out the cell walls now-connected via tape, and laminate another layer of tape on the other side, forming compliant hinges at the four corners of an active cell. We cut out the cell-wall component from extra tape.

As seen in (Figure 8b), We fabricate our airbags using polyethylene bags. commonly used for storing vacuum-sealed food (Foyo Sous Vide Vacuum Sealer Bags), since they are highly durable and made for heat sealing. After measuring and marking an airbag's silhouette, we use an impulse sealer (Metronic Impulse Sealer 8 inch) to seal the long edges, and manually seal the inward corners using a heat-controlled soldering iron. To avoid sticking in the latter process, we use a thin sheet of parchment paper between the iron and the plastic. Note that machine-controlled heat-sealing (e.g., [23, 33]) would also work for our airbags.

We attach the tubing component to the airbag using hot melt glue. To ensure air-tightness, we inject hot glue into the airbag opening where the tubing is attached.

We 3D print the scissor mechanism previously illustrated in Figure 5, including the two scissor leg components and the four snap-fit joints. We use a consumer-grade 3D printer (Tenlog Tl-D3 Pro) and print the parts with PLA (Polylactic Acid) filament. Figure 8c illustrates the assembly process of different components forming an active cell. We attach the airbag component and snap-fit component to the cell-wall component via a cyanoacrylate adhesive (GH1200), informed by engravings on the cell walls. Afterwards, we attach the scissor mechanism to the active cell with the snap-fit joints.

3.4.2 Passive lattice and passive cell fabrication. As shown in Figure 9, the passive lattice consists of flexible joints and rigid edges. We 3D print the joints using Ninjaflex TPU 85A, and laser-cut the edges from 3 mm acrylic sheets. Passive rigid cell inserts are 3D printed using PLA.

4 TECHNICAL EVALUATION

In this section, we characterize our active cells. We measure four main properties. (1) We characterize the actuation accuracy of a single cell. Confirming that an active cell can accurately deform to a target angle is the foundation of our robotic material. (2) Since active cells are embedded in a lattice, we evaluate the strength of one active cell in the context of how much it can move lattices of varying sizes that it is embedded in. To move larger lattices, we experiment with incrementing the number of active cells in a 7 x 7 lattice. We find adding more active cells to be able to overcome resistance in a larger lattice. (3) We further assess an active cell's performance to drive a lattice with varying numbers of rigid cells. Lastly, (4) we evaluate the accuracy with which our motion paths are reproduced by our metamaterial. We find that across the 7 paths we tested, the mean error is at 3.55%. We used 30 psi air pressure throughout our experiments. We note that these tests are intended to enable replicability of our *research prototypes*. As is typical in research, achieving product-readiness will require additional engineering, professional manufacturing, and quality control.

4.1 Single cell actuation accuracy

We aim to assess the actuation accuracy of a single unloaded active cell. We show the setup and results in Figure 10. We actuate the cell starting from $90°$ to target angles between $40°$ and $140°$ in increments of $10°$. We empirically determined this range to be most effective for our cells due to its construction and embedding of sensors and airbags in its interior. The results show a very high actuation accuracy of our unloaded active cell with a mean error of only 0.45% over the actuation range of $100°$.

4.2 Actuation strength within lattice

After verifying that our active cell can actuate itself accurately, we characterize its performance within the lattice. The lattice adds resistance through its mass, friction with surfaces, and gravity. In this experiment, we characterize an active cell's performance in actuating lattices of different sizes.

We use 6 different lattice sizes, i. e., 2×2, 3×3, 4×4, 5×5, 6×6, and 7×7. Each lattice is initially laid out in its default position, with the active cell being initialized at $90°$ and the remaining passive cells laid out manually at approx. $90°$. We drive each lattice by a single active cell located at the lower left corner. We actuate the active cell to the maximum to find the largest angle that the cell can still actuate within the respective lattices. The results presented in Figure 11 show that the max. angle reached by a single cell decreases with growing lattice size, as expected. While the max. angle within a 2×2 lattice is $138°$, it decreases to $115°$ for the 7×7 lattice.

We performed the same experiment, but on lattices hanging vertically, since we expect the impact of gravity to be higher than the impact of friction. Here, the active cell is located in the top left
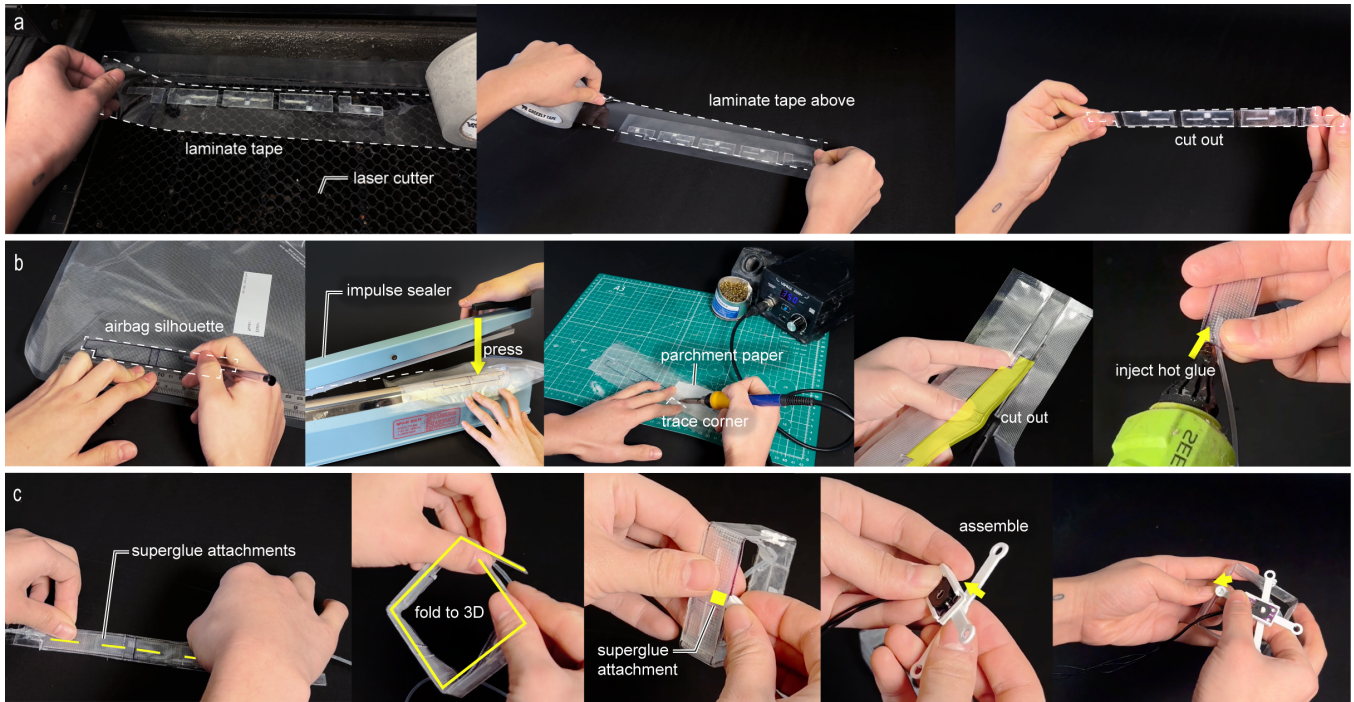
Figure 8: (a) We first laser cut cell walls with engravings to inform attachments, and laminate tape on both sides before cutting the cell-wall component out. (b) To make an airbag, we first draw the silhouette of an airbag, and use both an impulse sealer and a soldering iron to seal along its silhouette. After which we cut out the airbag. We use Silpoxy to attach two different-sized silicone tubes, and then use hot glue to hold the thinner tube in the airbag's opening. (c) To assemble the active cell, we attach an airbag component and 3D-printed snap-fit joints to the cell-wall component using superglue, and attach the scissor sensing mechanism to the cell via the snap-fit joints.
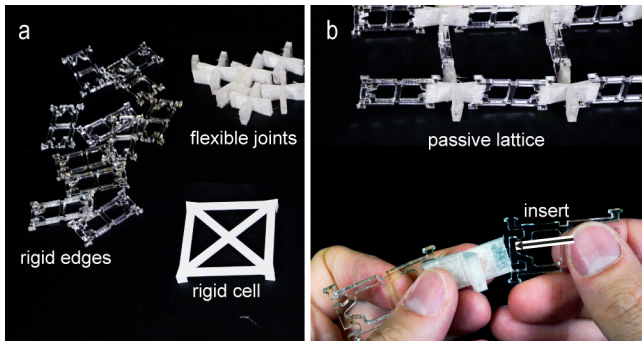

Figure 9: (a) We 3D-print flexible joints and passive rigid cell inserts, and laser-cut rigid edges from acrylic sheets. (b) To fabricate the passive lattice, we insert rigid edges into the flexible joints.

Figure 10: The actuation accuracy of a single active cell yields a mean error of only 0.45%.

corner, from where it attempts to lift the entire lattice. As we show in Figure 12, our active cell reaches max. 133° in the 2 × 2 and 110° in the 7 × 7 lattice.

We expected that a single active cell wouldn't be able to fully actuate given the resistance of larger lattices. Conversely, we assume th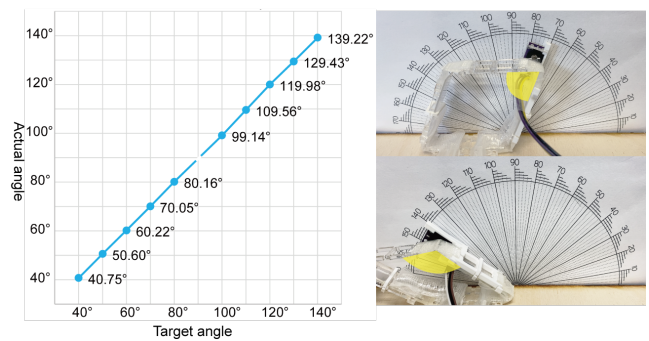at adding more active cells into the lattice will allow them to deform to larger angles. To confirm this assumption, we actuated our 7 × 7 horizontal lattice using first 1, then 2, 3, and 4 active cells placed along its diagonal, as shown in Figure 13. Our results validate that indeed more active cells can drive larger lattices, as their max. angle increases from 115° to 124°. Note that the 3rd active cell seems to be an outlier with a max. angle of 136°. This is likely due to differences in the construction of the handmade active cells
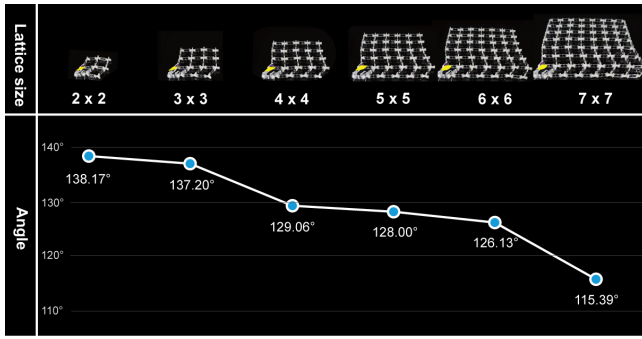
Figure 11: A single active cell can actuate a lattice of different sizes, but the max. angle reduces with the higher mass of the lattice, as expected.
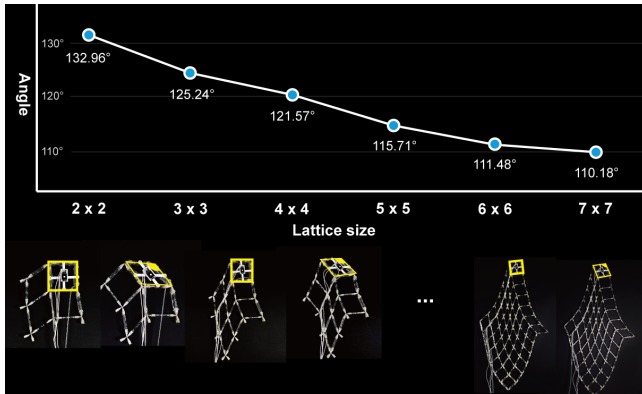

Figure 12: On vertically oriented lattices, the force required to overcome the mass and gravity is higher than in horizontal orientations. While one active cell can actuate a range of 1 to 48 cells, the maximum actuation range decreases as expected.

and/or the differences in the prototypical hardware we use (e. g., valves).

4.3 Influence of rigid cells

The lattice of passive shearing cells adds resistance, as we established. In this experiment, we aim to investigate the resistance that rigid cells introduce. We use a 3×3 lattice and place one active cell in the center. We add one rigid cell incrementally and measure the actuation accuracy within a range of 45° to 135°, with 15° increments. Figure 14 shows that 26 out of 30 angles were reached accurately. The two angles that were not reached are the extreme angles when all 4 rigid cells are in place. Additionally, the 45° angles for 2 and 3 rigid cells were not achieved either. This is because the lattice is anchored at the bottom left, which means that the active cell needs to pull more cells as they 'overhang' on the right side of the lattice. Rigid cells have the purpose of propagating and/or redirecting forces through the lattice, meaning that the motion of the active cells affects more cells at once. Therefore, increasing the number of rigid cells, and therefore decreasing the number of degrees of freedom, require more force to be effective. This can be
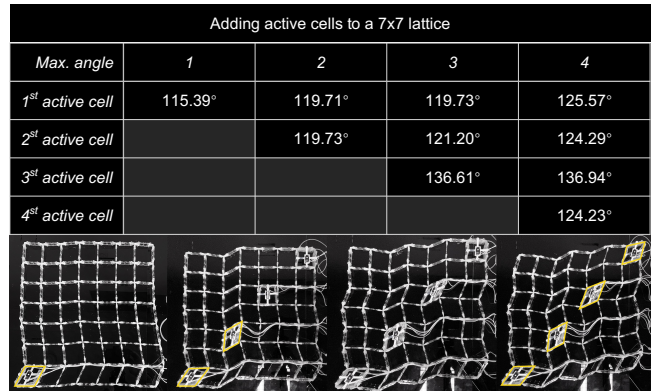
Adding active cells to a 7x7 lattice				
Max. angle	1	2	3	4
1ˢᵗ active cell	115.39°	119.71°	119.73°	125.57°
2ˢᵗ active cell		119.73°	121.20°	124.29°
3ˢᵗ active cell			136.61°	136.94°
4ˢᵗ active cell				124.23°

Figure 13: The max. achievable angle of our active cells increases when using multiple to drive the 7×7 horizontal lattice. For example, the max. angle of the first active cell increases from 115.39° with only one active cell to 125.57° with four active cells. This indicates that the increasing resistance of larger lattices can be overcome by adding more active cells.

achieved by adding multiple active cells, as all of our applications do. Additionally, we cap the angle range at 60° to provide reliable results to users. Note that all application examples demonstrated in this paper did not require such extreme angles or constraints.

4.4 Path actuation accuracy

To evaluate how well our robotic metamaterial approximates desired motion paths, we tested using 7 different target paths, as illustrated in Figure 15: a horizontal line (P1), vertical line (P2), horizontal arc (P3), vertical arc (P4), triangle (P5), rectangle (P6), and zigzag path (P7). We chose a mix of basic paths (lines, arcs) in different directions, as well as compound paths (triangle, rectangle,

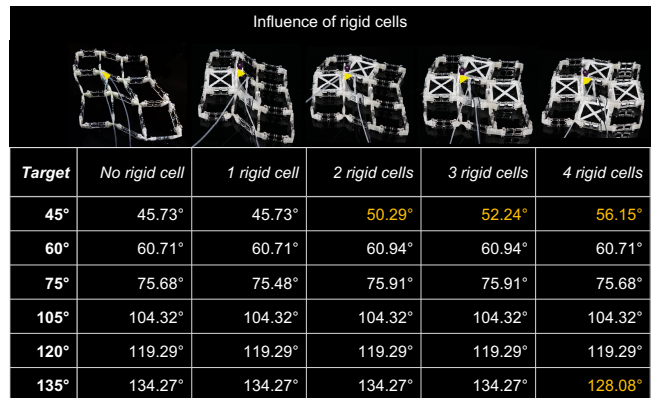|	Influence of rigid cells				
Target	No rigid cell	1 rigid cell	2 rigid cells	3 rigid cells	4 rigid cells
45°	45.73°	45.73°	50.29°	52.24°	56.15°
60°	60.71°	60.71°	60.94°	60.94°	60.71°
75°	75.68°	75.48°	75.91°	75.91°	75.68°
105°	104.32°	104.32°	104.32°	104.32°	104.32°
120°	119.29°	119.29°	119.29°	119.29°	119.29°
135°	134.27°	134.27°	134.27°	134.27°	128.08°

Figure 14: We show how increasing the number of rigid cells in the lattice increases its stiffness which impacts the actuation range of the active cell. The cell achieves 26 out of 30 target angles accurately.

zigzag) to observe the accuracy at different features, such as corners. Using our computational design tool, we generated *one* 4×4 material configuration to draw *all* 7 paths (Figure 15), along with the angles to control each path. We actuated each path 10 times and video-recorded the trial. We coded the physical path and computed the error to the target path like Ion et al. [13], i. e., we calculate the error as the sum of the point-wise Euclidean distances between the target and the actual paths and normalize it with respect to the length of the paths.

Our results, shown in Figure 15, show that the output of our robotic metamaterial can approximate 7 different paths within the same material configuration with a very good mean accuracy of 3.55%. The most accurate path has a mean error of 1.97% and the least accurate 5.39%. The least accurate path is the vertical line (P2), which is consistently tilted. Based on our experiment, it seems to be due to the difference in the opening speeds of our valves. Our active cells produce inherently arched paths (pulling to the left in this setup), and the active cell that should counter this arched motion is actuated a little later based on the slower valve speed. Based on this observation, we measured the opening speed of our valves and found considerable differences of up to 1.4 ms of an average opening speed of 4.6 ms. The overall good accuracy results of our system indicate that our system can be polished further by using better (non-prototypical) hardware and manufacturing.

Summary. Overall, our experiments confirm our design goals and expectations. The active cell itself can actuate to target angles effectively within the ranges of $40°$ to $140°$. When embedded in a 6×6 lattice, it is still strong enough to move 35 (6×6 - 1) horizontal cells to over $120°$, which is a sufficient range for our demonstrated applications. In a vertical setup, the cell can overcome gravity and still move 15 other cells within that range. Adding more rigid cells introduces additional constraints into the lattice, thereby increasing resistance and requiring the use of more active cells. Lastly, our robotic metamaterial shows a good accuracy of 3.55% on average over 7 different paths actuated with the same material configuration. Additionally, we believe that high-end hardware and industrial precision manufacturing can improve accuracy in the future.

5 SOFTWARE IMPLEMENTATION

Understanding how to compose flexible and rigid passive cells, with active cells, to achieve a particular purpose, requires specialized knowledge and can be difficult. To assist users in designing their robotic metamaterials, we offer an inverse design tool for users, as shown in Figure 20a. This tool allows a user to specify a set of desired motions in a 2D plane, and then uses an optimization algorithm to find a configuration of cells that can closely approximate that motion. This allows a designer to specify *what* results they desire, without working out *how* to achieve that result. This eliminates the need, for example, to understand the complexities of how the motion of one active cell propagates through other rigid or flexible cells, or how the motion of one cell combines with that of another.

To achieve this, our tool extends the algorithm presented in [13], which we expand to support active cells and multiple motion paths within 2D materials as described in this paper. We give a visual overview of the previous algorithm in Figure 16a and our extensions in (b).

Background. The previous algorithm presented in [13] takes a user-defined empty lattice and two motion paths as input, i. e., one input and one output path, since the algorithm was designed to generate a metamaterial mechanism that transforms the input into the output path. The result of the algorithm is a generated *passive* metamaterial consisting of rigid and shearing cells approximating the user-defined paths. It uses a traditional iterative optimization loop, which first generates a cell placement of rigid cells within the lattice, for which they used Simulated Annealing. The algorithm then simulates the movement of the cell configuration using a custom kinematics simulation using IPOPT [35]. It evaluates the error between the user-defined (gray) path in Figure 16(a2) and the path produced by the current cell configuration (blue). If the error is lower than a specified max. error, the algorithm returns the passive cell placement for the mechanism to the user. If the error is too high, the algorithm returns to the optimization step and proceeds iteratively. To reduce the combinatorial search space, the algorithm also modeled the parallelism constraints of opposing cell edges to build a constraint graph (Figure 16(a1)). The connected components within this graph model the DoF in the cell configuration, which is used in the optimization to generate mechanically unique cell configurations by merging or splitting the connected components.

Our extension. We keep these parts, but extend them to (1) allow users to define multiple target paths that should be achievable with the same cell placement to implement different robotic functions, by actuating the same configured cell grid in different ways. Subsequently, (2) we place active cells, such that users can actuate the material after fabrication.

(1) Multiple motions from the same configuration. To allow users to control different functions using a single lattice we need to generate cell placements that can achieve multiple separately actuated motions (e. g., in the desktop notifier example following in Section 6). In our extended algorithm, we allow users to specify multiple paths when initializing the optimization process, each path corresponds to one of the separate motions. During optimization, these are treated as separate lattices to optimize, though we ensure that the same configuration is always used for all lattices by using a common working configuration at each simulated annealing iteration. Based on Ion et al., we calculate the path error ε as the sum of the differences between all user-defined target paths and their corresponding path currently produced by the lattice. In addition to the path error ε, our objective also penalizes the number of degrees of freedom N_{AC}, since the number of degrees of freedom corresponds to the number of active cells needed to be placed, as we describe in the following.

(2) Active cell placement optimization. Our second major extension is optimizing the placement of active cells within a robotic metamaterial. Since our main goal is to enable robotic motion, we need to achieve a well-defined motion on the lattice. To achieve this, we first run the original algorithm to place as many rigid cells as possible. The result will be a grid with multiple degrees of freedom (2 - 5 DoF per [13]), depending on the path complexity. The key insight is to place active cells at positions that remove degrees of freedom, i. e., where they merge connected components on the constraint graph. This is possible because active cells perform the
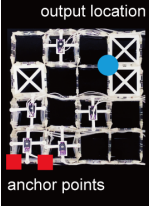
		Path 1	Path 2	Path 3	Path 4	Path 5	Path 6	Path 7
Accuracy visualization								
Trials	1	3.24%	3.92%	2.15%	2.50%	4.13%	3.23%	2.53%
	2	4.85%	6.58%	1.64%	1.12%	3.95%	2.13%	1.99%
	3	5.51%	4.58%	2.55%	1.67%	2.97%	2.07%	3.34%
	4	4.92%	6.72%	3.13%	2.82%	4.46%	3.69%	5.18%
	5	1.47%	3.88%	3.08%	5.58%	2.68%	3.30%	4.41%
	6	4.26%	6.16%	1.38%	3.12%	3.58%	2.19%	6.71%
	7	1.76%	5.42%	1.06%	3.37%	4.13%	2.02%	3.91%
	8	4.34%	5.55%	0.95%	5.09%	2.68%	2.64%	4.50%
	9	4.84%	7.13%	1.33%	2.74%	4.70%	2.82%	3.77%
	10	2.94%	3.95%	2.39%	2.80%	6.27%	2.13%	3.58%
Mean		3.81%	5.39%	1.97%	3.09%	3.96%	2.62%	3.99%
SD		1.32%	1.18%	0.76%	1.29%	1.02%	0.57%	0.57%

Figure 15: We used one Robotic Metamaterial configuration to approximate 7 distinct paths. Target paths are visualized in light gray. We approximated each path for 10 times, the material's motion paths are visualized in blue. Resulting error rates are mostly below 5%, indicating our Robotic Metamaterial is capable of following custom paths.
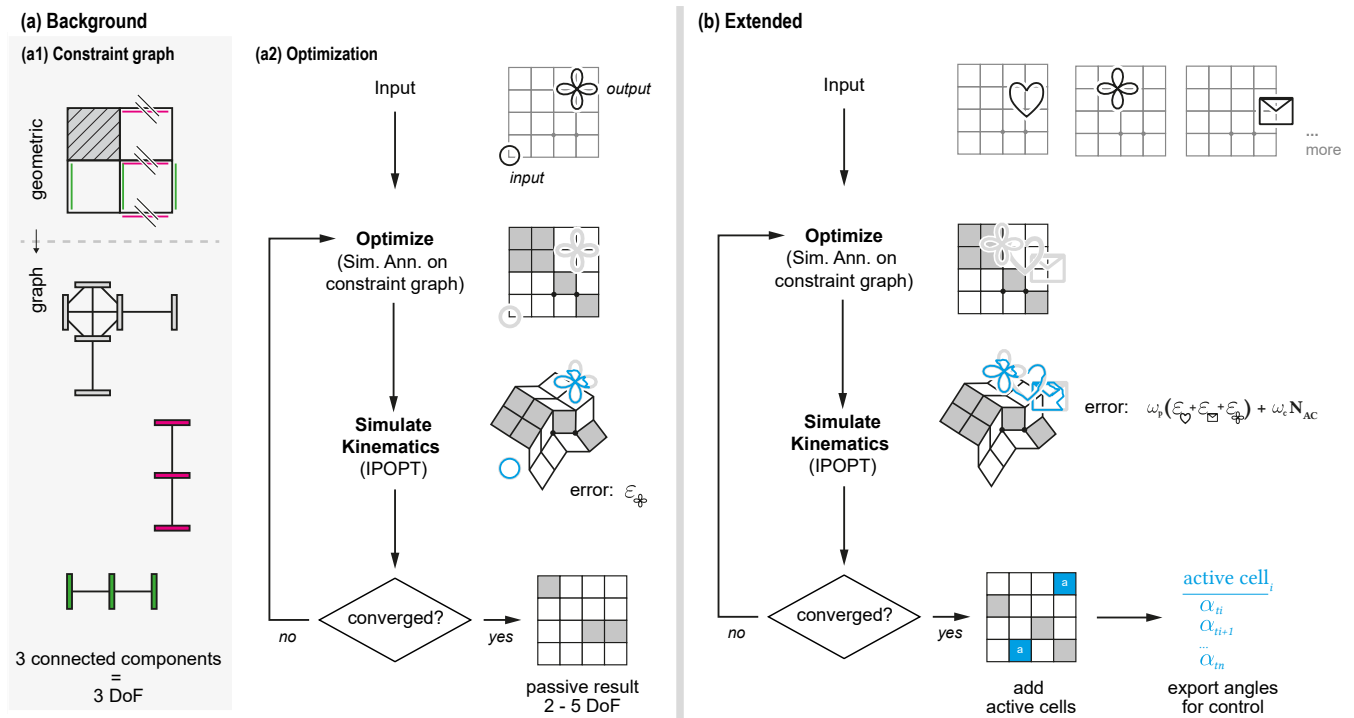

Figure 16: A visual overview of our inverse design software. We extend (a) the algorithm by Ion et al. [13] by (b) optimizing for multiple paths and placing active cells for actuating the metamaterial.

same way as rigid cells in that they drive the edges within their connected component, just not necessarily at a 90° angle. After having merged all connected components, we simulate the mechanism and record the angle sequence at each active cell. Our control loop for the physical cells reads these angles to actuate the material according to the users' design.

Relationship between reachable space & number of actuators. Our main objectives are to minimize (1) the path error shown as ε in Figure 16b and (2) the complexity of assembly, which is governed

by the number of active cells (N_{AC} in Figure 16b) to be placed in the physical lattice. A lower number of active cells typically requires more rigid cells and tends to produce lower path accuracy as its reachable area decreases. This is a trade-off that users can steer. Depending on the application, users might want to keep assembly effort low and can do with a less accurate result. In other applications, users might need to get the path completely accurate and will be willing to use many active cells. In Figure 17, we illustrate results for 2 different example target paths across different complexity settings.

vertex as the target path and optimize the cells that approximate it. We sampled 4 different output locations on a 3×3, 4×4, and 5×5 lattice, respectively (shown in Figure 18), including 1 location in the center, and 3 locations in the corner of the lattice. The results give insight into how different locations on the material can cover different moving areas of the material. The results also confirm that the further the output location is from the anchor points, the greater the reachable workspace, and that larger lattices allow for a larger reachable workspace.

Figure 18: The reachable workspace of four different output locations on the 3×3, 4×4, and 5×5 lattice. Each output location on the material exhibits a different range of motion, while a larger lattice allows a larger reachable workspace.
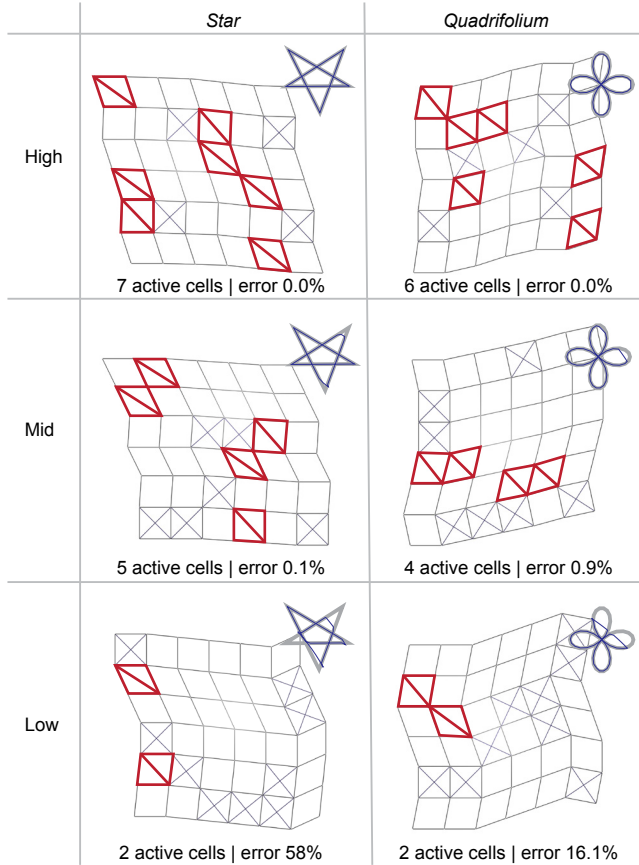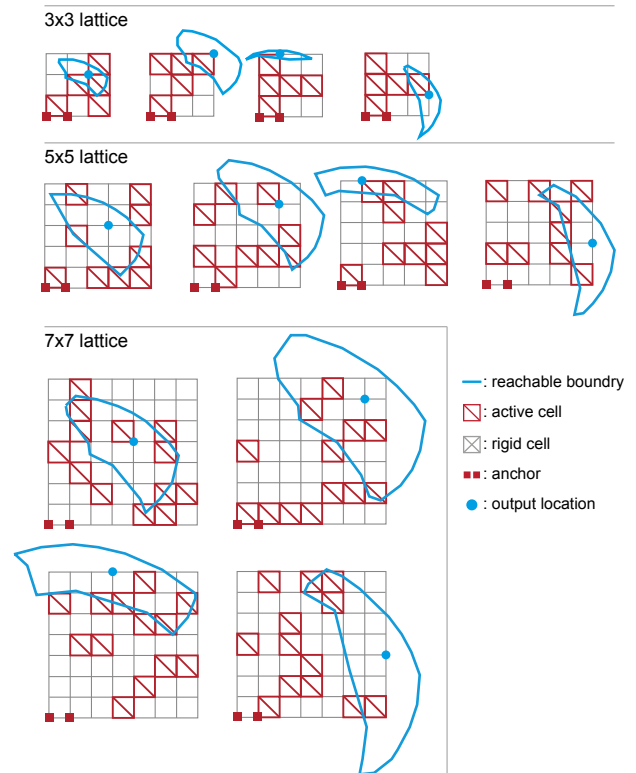

Figure 17: Illustration of the trade-off between accuracy and number of active cells for the example of two abstract paths and three resolutions. The paths in blue show the achieved motion path of the structure, and the gray path in the background shows the target path. We highlight the actuated cells in red. The error is relative to the target path's length.

Generally, understanding what motions a given lattice is able to perform is difficult due to the constraints that cells impose on each other. Ion et al. [13] initiated this discussion by reasoning how the scale of a path relates to its distance to the anchors, with larger distances allowing for longer paths. To provide more insight into this, we simulated the maximum reachable workspace of different vertices within materials of different sizes, as shown in Figure 18. To generate this workspace, we simply use a large circle around the

To provide insights into the impact of active vs rigid cells – and therefore of DoF in the system – we simulated the reachable workspace of a 5×5 lattice with an increasing number of active cells from 1 to 6, shown in Figure 19. The results show how more active cells in the material provide a larger motion range for the same output location.

6 APPLICATION EXAMPLES

In the following, we explore the utility of our Robotic Metamaterials as a modular robotic platform for users. We have already demonstrated our robotic material as a custom robotic theater in an educational context in Figure 3. This application highlighted the
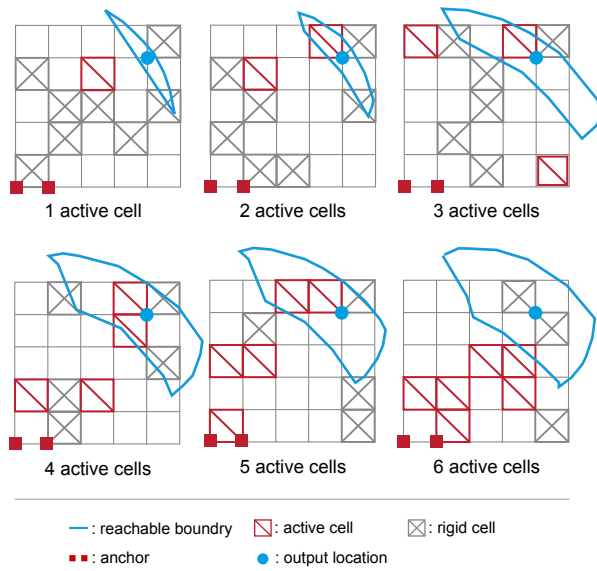
Figure 19: The reachable workspace depending on varying active cells from 1 to 6 within a 5 × 5 lattice. Adding more active cells increases the workspace for the same output location.

(re)configurability of our material, its modularity, and hands-on programming of the desired through manual demonstration of a movement by users. The theater application also highlighted how multiple layers of our material can work together. In addition, we illustrate example applications that capture e. g., traditional robotic functions, such as locomotion, that can be integrated into the built environment, such as walls, or can be integrated into furniture, e. g., desks. The major benefit of our approach is that through its modularity it enables non-expert users to build *all* application examples in this section hands-on and in-situ.

6.1 Integrated desktop notifications

In this application example, we explore how Robotic Metamaterials can be integrated into furniture and interact with users. Figure 20 shows an example where users configure material to output symbols as haptic notifications. Here, the user has chosen to program the material with a heart or a water drop symbol. The heart symbol notifies them that their partner messaged them and the water drop to drink water. The symbols provide a haptic or visual display which is drawn using a small rod moving under an elastic fabric in contact with the user's skin (or seen by the user to be moving).

Since these symbols are complex and rendered on a larger lattice (here 5 × 5), it is not obvious where to place rigid or active cells to create a well-defined mechanism. For this, we show in Figure 20a how users design the robotic material using our computational design tool (described in Section 5). Users provide their desired paths as input to the software, which optimizes the placement of rigid and active cells, and generates the control code to drive the material. After users place the cells accordingly (b), they can interact with the material through the desk (c). Note that all symbols are
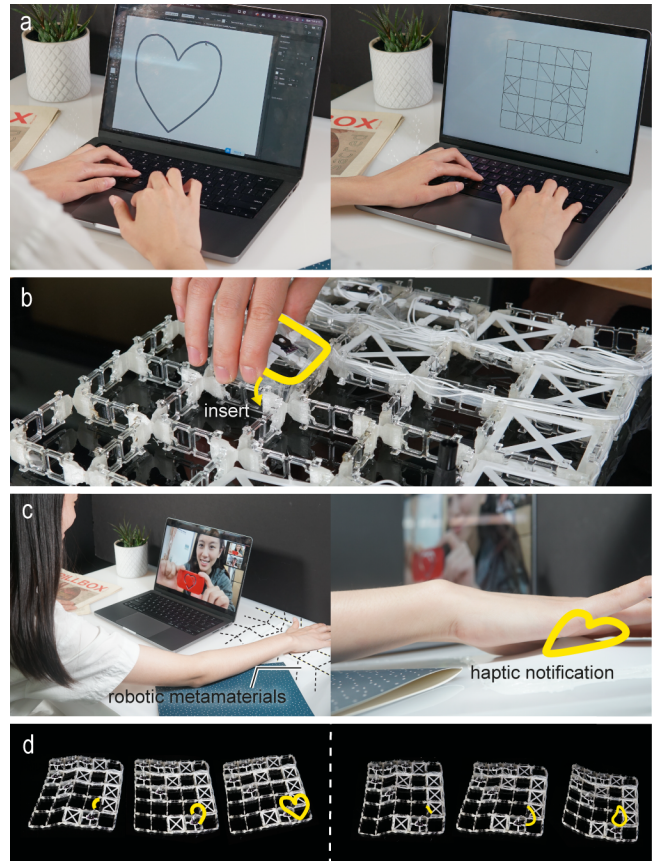

Figure 20: (a) A user designs a heart path for their haptic notification, and receives cell configuration from our software. (b) They insert cells as shown in the software. (c) When video-chatting with a friend, Robotic Metamaterials integrated into their desk renders a heart shape on their palm. (d) The same Robotic Metamaterials configuration is able to draw other symbols, such as a water drop.

rendered with the same cell configuration, i. e., one configured Robotic Metamaterial can render multiple distinct functions.

After using the notifications for a while, users decide to add a notification to wake them from power naps, as we illustrate in Figure 21. They choose to render 3 quick taps, for which they use the input function of our material, grab the end-effector, and program the material by demonstrating the motion manually. This illustrates how users can choose whether to use our design tool, which is most suitable for complex and/or compound motions, or to simply define motions hands-on in-situ by demonstration, which is best for simple paths.

6.2 Robot locomotion

In Figure 22, we show how our robotic metamaterial platform can implement conventional robotic functions, specifically locomotion. We demonstrate a crawling robot made from our Robotic Metamaterial. It demonstrates that a small patch of material—here 4 × 2 cells—augmented with two active and two rigid cells can implement
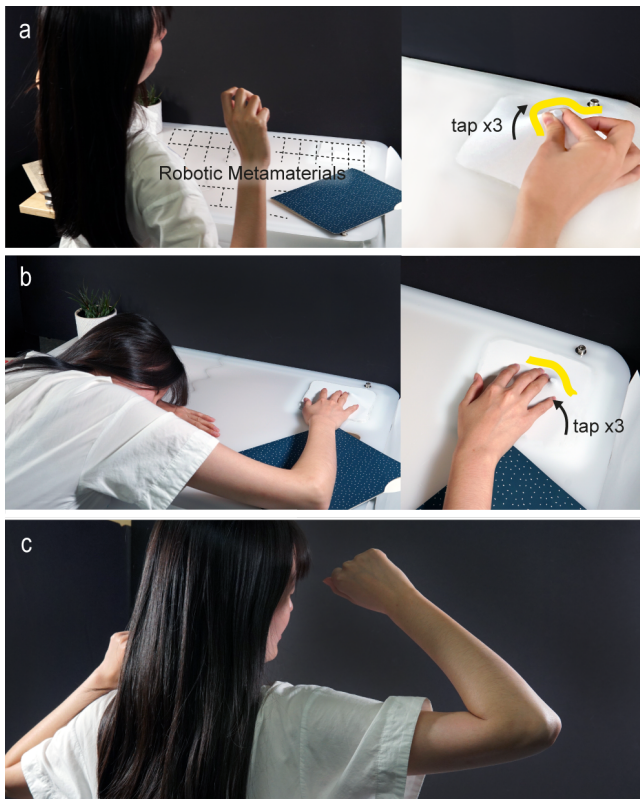
Figure 21: (a) A user wants a haptic alarm to wake up from a power nap. She grabs a vertically extending element attached to the Robotic Metamaterial integrated into the desk, and records three taps. (b) The user sleeps on the desk. The material taps the user with their recorded motion. (c) The user wakes up.
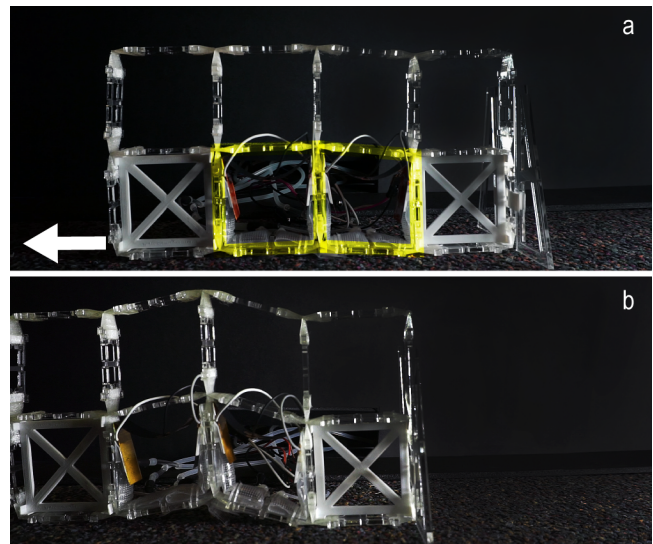
Figure 22: We show a compliant crawling robot made out of a 2×4 grid using two active cells and two rigid cells. Users clip on legs to provide differential friction. We annotate the active cells in yellow.

useful devices. The two active cells in the center move the crawler up. We 3D print feet to clip onto our cells to give the crawler differential friction. This represents a small trade-off—it makes the material simpler, lowers assembly effort, and reduces the number of actuators needed, but introduces a specialized part. Given this simplification, an expert user may not need to use our design tool for configuring the above locomotion, but the design tool remains an option for novice users (i.e., who may not be able to add the specialized part), or for configuring the material to perform more complex locomotion.

6.3 Robotic wall material

Figure 23 shows a wall-mounted Robotic Metamaterial platform. The user decides to use it as a programmable light source for their soldering station. They move the material to program the light to point to where they place their components. They also program it to point to their tools and the water bottle individually. The light source is mounted onto a Stewart platform, a common motion platform mechanism. We connect the platform to our shear cells through scissor mechanisms. As the cell shears, its diagonal shortens and pushes the ends of the scissor mechanism together, which

lengthens the scissor mechanism and tilts the platform to direct the light. With an understanding of how the material would need to move to actuate the scissor mechanism, the user can leverage our design tool to configure the material.

Our prototype aims to illustrate how such materials can be used in the built environment. While our prototype is a 3×3 lattice, we envision that entire walls can be augmented with our lattice and users can reversibly break connections in the lattice selectively to create functional groups that can be configured with active cells. Such built environments can then also provide a tighter integration with tracking capabilities. In such complex cases, our design tool would be extremely useful in aiding the prototyping of these new interactions.

Note that we did not implement automatic triggers for our research prototypes at this stage. Given the computer-controlled nature of our metamaterial, connecting our applications with data input, such as tracking, timers, calendars, etc., would be trivial after enhancing our control circuit with wireless communication modules, e.g., Wifi or Bluetooth.

7 CONCLUSION

In this paper, we presented a novel actuated material based on metamaterial mechanisms. The material can offer shape-changing and robotic capabilities and high customizability, while being modular. We demonstrated its potential by illustrating distinct application scenarios, including furniture-integrated robotic materials that can interact with the user physically, creative applications such as a physical theater, or traditional robotic functions like locomotion. We believe that this material presents a first step towards user-configurable complex robotic materials. The research prototypes demonstrated in this paper allowed us to explore the utility and
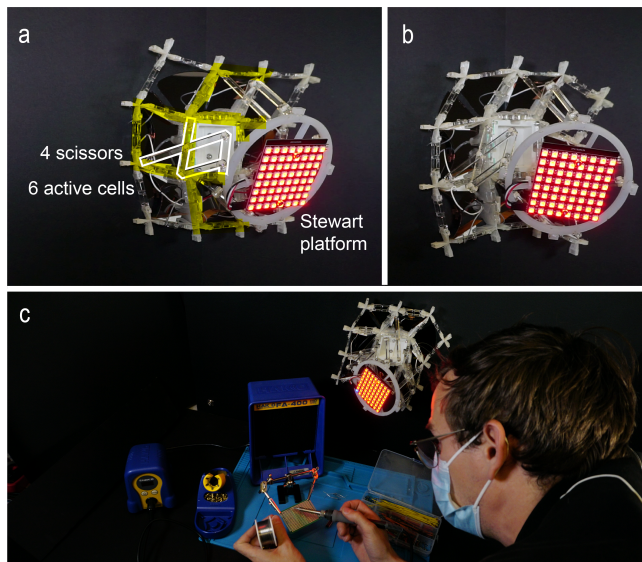
Figure 23: We demonstrate our robotic materials as wall-mounted robotic platforms. Here, we (a) attach a light source on a Stewart platform that (b) directs the light to (c) illuminate users soldering tasks.

interaction with such materials in the future. The limitations of our current implementation include laborious fabrication of the active cell, which due to its manual nature can lead to inconsistencies in cell performance. However, an industrial process can alleviate such issues in the future. Additionally, the need for an air supply and the currently large valves are a limitation right now, albeit typically acceptable for research projects.

Our vision for this project goes far beyond our current implementation, and towards miniaturized robotic metamaterials to *span the continuum between materials and robots*. One example could be a robot that is specifically made for disaster area exploration. It can be configured to walk, crawl, fold, and roll through cavities, or even implement material properties such as damping [32]. All these functions could be integrated into the passive material ad-hoc and controlled remotely. Miniaturization is a big challenge. However, we did design it with miniaturization potential in mind. The air pockets could be included in a layer-based lamination process, based on evidence of the fabrication of small-scale pneumatic or hydraulic pockets [16]. The most challenging components to integrate are the valves and air supply. Here again recent work on layer-based valve systems [6, 26] point towards feasibility for mass-fabricable, small-scale valves to integrate in our metamaterial. Lastly, integrating the air supply might be possible in the future through developments in small-scale pumps (e.g., Piezoelectric Pumps[2]).

While investigating future technologies is always challenging, we believe that this paper brings us closer to understand how such robotic metamaterials can be relevant to users and how they might interact with them.

---

[2]https://www.piezodata.com/precision-piezoelectric-air-pump/

REFERENCES

[1] Katia Bertoldi, Vincenzo Vitelli, Johan Christensen, and Martin Van Hecke. 2017. Flexible mechanical metamaterials. *Nature Reviews Materials* 2, 11 (2017), 1–11.

[2] Shanshan Chen, Zhiguang Liu, Huifeng Du, Chengchun Tang, Chang-Yin Ji, Baogang Quan, Ruhao Pan, Lechen Yang, Xinhao Li, Changzhi Gu, et al. 2021. Electromechanically reconfigurable optical nano-kirigami. *Nature communications* 12, 1 (2021), 1–8.

[3] Kyung Yun Choi and Hiroshi Ishii. 2021. Therms-Up!: DIY Inflatables and Interactive Materials by Upcycling Wasted Thermoplastic Bags. In *Proceedings of the Fifteenth International Conference on Tangible, Embedded, and Embodied Interaction (TEI '21)*. Association for Computing Machinery, New York, NY, USA, 1–8. https://doi.org/10.1145/3430524.3442457

[4] Zhitong Cui, Shuhong Wang, Junxian Li, Shijian Luo, and Alexandra Ion. 2023. MiuraKit: A Modular Hands-On Construction Kit For Pneumatic Shape-Changing And Robotic Interfaces. In *Proceedings of the 2023 ACM Designing Interactive Systems Conference*. 2066–2078.

[5] Jun Gong, Olivia Seow, Cedric Honnet, Jack Forman, and Stefanie Mueller. 2021. MetaSense: Integrating Sensing Capabilities into Mechanical Metamaterial. In *The 34th Annual ACM Symposium on User Interface Software and Technology* (Virtual Event, USA) *(UIST '21)*. Association for Computing Machinery, New York, NY, USA, 1063–1073. https://doi.org/10.1145/3472749.3474806

[6] Jesse T. Gonzalez and Scott E. Hudson. 2022. Layer by Layer, Patterned Valves Enable Programmable Soft Surfaces. *Proc. ACM Interact. Mob. Wearable Ubiquitous Technol.* 6, 1, Article 12 (mar 2022), 25 pages. https://doi.org/10.1145/3517251

[7] Daniel Groeger and Jürgen Steimle. 2019. LASEC: Instant Fabrication of Stretchable Circuits Using a Laser Cutter. In *Proceedings of the 2019 CHI Conference on Human Factors in Computing Systems* (Glasgow, Scotland Uk) *(CHI '19)*. Association for Computing Machinery, New York, NY, USA, 1–14. https://doi.org/10.1145/3290605.3300929

[8] Elliot W. Hawkes, Laura H. Blumenschein, Joseph D. Greer, and Allison M. Okamura. 2017. A soft robot that navigates its environment through growth. *Science Robotics* 2, 8 (July 2017), eaan3028. https://doi.org/10.1126/scirobotics.aan3028 Publisher: American Association for the Advancement of Science.

[9] Liang He, Gierad Laput, Eric Brockmeyer, and Jon E. Froehlich. 2017. Squeeza-Pulse: Adding Interactive Input to Fabricated Objects Using Corrugated Tubes and Air Pulses. In *Proceedings of the Eleventh International Conference on Tangible, Embedded, and Embodied Interaction* (Yokohama, Japan) *(TEI '17)*. Association for Computing Machinery, New York, NY, USA, 341–350. https://doi.org/10.1145/3024969.3024976

[10] Liang He, Huaishu Peng, Michelle Lin, Ravikanth Konjeti, François Guimbretière, and Jon E. Froehlich. 2019. Ondulé: Designing and Controlling 3D Printable Springs. In *Proceedings of the 32nd Annual ACM Symposium on User Interface Software and Technology* (New Orleans, LA, USA) *(UIST '19)*. Association for Computing Machinery, New York, NY, USA, 739–750. https://doi.org/10.1145/3332165.3347951

[11] Alexandra Ion, Johannes Frohnhofen, Ludwig Wall, Robert Kovacs, Mirela Alistar, Jack Lindsay, Pedro Lopes, Hsiang-Ting Chen, and Patrick Baudisch. 2016. Metamaterial Mechanisms. In *Proceedings of the 29th Annual Symposium on User Interface Software and Technology* (Tokyo, Japan) *(UIST '16)*. Association for Computing Machinery, New York, NY, USA, 529–539. https://doi.org/10.1145/2984511.2984540

[12] Alexandra Ion, Robert Kovacs, Oliver S. Schneider, Pedro Lopes, and Patrick Baudisch. 2018. Metamaterial Textures. In *Proceedings of the 2018 CHI Conference on Human Factors in Computing Systems* (Montreal QC, Canada) *(CHI '18)*. Association for Computing Machinery, New York, NY, USA, 1–12. https://doi.org/10.1145/3173574.3173910

[13] Alexandra Ion, David Lindlbauer, Philipp Herholz, Marc Alexa, and Patrick Baudisch. 2019. Understanding Metamaterial Mechanisms. In *Proceedings of the 2019 CHI Conference on Human Factors in Computing Systems* (Glasgow, Scotland Uk) *(CHI '19)*. Association for Computing Machinery, New York, NY, USA, 1–14. https://doi.org/10.1145/3290605.3300877

[14] Alexandra Ion, Ludwig Wall, Robert Kovacs, and Patrick Baudisch. 2017. Digital Mechanical Metamaterials. In *Proceedings of the 2017 CHI Conference on Human Factors in Computing Systems* (Denver, Colorado, USA) *(CHI '17)*. Association for Computing Machinery, New York, NY, USA, 977–988. https://doi.org/10.1145/3025453.3025624

[15] Roderic Lakes. 1987. Foam structures with a negative Poisson's ratio. *Science* 235 (1987), 1038–1041.

[16] Qiuyu Lu, Jifei Ou, João Wilbert, André Haben, Haipeng Mi, and Hiroshi Ishii. 2019. MilliMorph – Fluid-Driven Thin Film Shape-Change Materials

for Interaction Design. In *Proceedings of the 32nd Annual ACM Symposium on User Interface Software and Technology* (New Orleans, LA, USA) *(UIST '19)*. Association for Computing Machinery, New York, NY, USA, 663–672. https://doi.org/10.1145/3332165.3347956

[17] Ramses V. Martinez, Carina R. Fish, Xin Chen, and George M. White-sides. 2012. Elastomeric Origami: Programmable Paper-Elastomer Composites as Pneumatic Actuators. *Advanced Functional Materials* 22, 7 (2012), 1376–1384. https://doi.org/10.1002/adfm.201102978 _eprint: https://onlinelibrary.wiley.com/doi/pdf/10.1002/adfm.201102978.

[18] Vittorio Megaro, Jonas Zehnder, Moritz Bächer, Stelian Coros, Markus Gross, and Bernhard Thomaszewski. 2017. A Computational Design Tool for Compliant Mechanisms. *ACM Trans. Graph.* 36, 4, Article 82 (jul 2017), 12 pages. https://doi.org/10.1145/3072959.3073636

[19] Bobak Mosadegh, Panagiotis Polygerinos, Christoph Keplinger, Sophia Wennstedt, Robert F. Shepherd, Unmukt Gupta, Jongmin Shim, Katia Bertoldi, Conor J. Walsh, and George M. Whitesides. 2014. Pneumatic Networks for Soft Robotics that Actuate Rapidly. *Advanced Functional Materials* 24, 15 (2014), 2163–2170. https://doi.org/10.1002/adfm.201303288 _eprint: https://onlinelibrary.wiley.com/doi/pdf/10.1002/adfm.201303288.

[20] Stefanie Mueller, Bastian Kruck, and Patrick Baudisch. 2013. LaserOrigami: Laser-Cutting 3D Objects. In *Proceedings of the SIGCHI Conference on Human Factors in Computing Systems* (Paris, France) *(CHI '13)*. Association for Computing Machinery, New York, NY, USA, 2585–2592. https://doi.org/10.1145/2470654.2481358

[21] Ryuma Niiyama, Xu Sun, Lining Yao, Hiroshi Ishii, Daniela Rus, and Sangbae Kim. 2015. Sticky Actuator: Free-Form Planar Actuators for Animated Objects. In *Proceedings of the Ninth International Conference on Tangible, Embedded, and Embodied Interaction*. ACM, Stanford California USA, 77–84. https://doi.org/10.1145/2677199.2680600

[22] Jifei Ou, Zhao Ma, Jannik Peters, Sen Dai, Nikolaos Vlavianos, and Hiroshi Ishii. 2018. KinetiX - designing auxetic-inspired deformable material structures. *Computers & Graphics* 75 (Oct. 2018), 72–81. https://doi.org/10.1016/j.cag.2018.06.003

[23] Jifei Ou, Mélina Skouras, Nikolaos Vlavianos, Felix Heibeck, Chin-Yi Cheng, Jannik Peters, and Hiroshi Ishii. 2016. AeroMorph - Heat-Sealing Inflatable Shape-Change Materials for Interaction Design. In *Proceedings of the 29th Annual Symposium on User Interface Software and Technology* (Tokyo, Japan) *(UIST '16)*. Association for Computing Machinery, New York, NY, USA, 121–132. https://doi.org/10.1145/2984511.2984520

[24] Johannes TB Overvelde, Twan A De Jong, Yanina Shevchenko, Sergio A Becerra, George M Whitesides, James C Weaver, Chuck Hoberman, and Katia Bertoldi. 2016. A three-dimensional actuated origami-inspired transformable metamaterial with multiple degrees of freedom. *Nature communications* 7, 1 (2016), 1–8.

[25] Romain Prévost, Emily Whiting, Sylvain Lefebvre, and Olga Sorkine-Hornung. 2013. Make It Stand: Balancing Shapes for 3D Fabrication. *ACM Trans. Graph.* 32, 4, Article 81 (jul 2013), 10 pages. https://doi.org/10.1145/2461912.2461957

[26] Bian Qian, Gareth H. McKinley, and A. E. Hosoi. 2013. Structure evolution in electrorheological fluids flowing through microchannels. *Soft Matter* 9 (2013), 2889–2898. https://doi.org/10.1039/C2SM27022F Issue 10.

[27] Thijs Jan Roumen, Willi Müller, and Patrick Baudisch. 2018. Grafter: Remixing 3D-Printed Machines. In *Proceedings of the 2018 CHI Conference on Human Factors in Computing Systems* (Montreal QC, Canada) *(CHI '18)*. Association for Computing Machinery, New York, NY, USA, 1–12. https://doi.org/10.1145/3173574.3173637

[28] Krishna Kumar Saxena, Raj Das, and Emilio P. Calius. 2016. Three Decades of Auxetics Research – Materials with Negative Poisson's Ratio: A Review. *Advanced Engineering Materials* 18, 11 (2016), 1847–1870. https://doi.org/10.1002/adem.201600053 arXiv:https://onlinelibrary.wiley.com/doi/pdf/10.1002/adem.201600053

[29] Christian Schumacher, Bernd Bickel, Jan Rys, Steve Marschner, Chiara Daraio, and Markus Gross. 2015. Microstructures to Control Elasticity in 3D Printing. *ACM Trans. Graph.* 34, 4, Article 136 (July 2015), 13 pages. https://doi.org/10.1145/2766926

[30] Lucas A Shaw, Samira Chizari, Matthew Dotson, Yuanping Song, and Jonathan B Hopkins. 2018. Compliant rolling-contact architected materials for shape reconfigurability. *Nature communications* 9, 1 (2018), 1–12.

[31] Robert F. Shepherd, Filip Ilievski, Wonjae Choi, Stephen A. Morin, Adam A. Stokes, Aaron D. Mazzeo, Xin Chen, Michael Wang, and George M. Whitesides. 2011. Multigait soft robot. *Proceedings of the National Academy of Sciences of the United States of America* 108, 51 (Dec. 2011), 20400–20403. https://doi.org/10.1073/pnas.1116564108

[32] Madlaina Signer, Alexandra Ion, and Olga Sorkine-Hornung. 2021. Developable Metamaterials: Mass-fabricable Metamaterials by Laser-Cutting Elastic Structures. In *Proceedings of the 2021 CHI Conference on Human Factors in Computing Systems*. 1–13.

[33] Saiganesh Swaminathan, Michael Rivera, Runchang Kang, Zheng Luo, Kadri Bugra Ozutemiz, and Scott E. Hudson. 2019. Input, Output and Construction Methods for Custom Fabrication of Room-Scale Deployable Pneumatic Structures. *Proc. ACM Interact. Mob. Wearable Ubiquitous Technol.* 3, 2, Article 62 (jun 2019),

17 pages. https://doi.org/10.1145/3328933

[34] Barry A. Trimmer, Ann E. Takesian, Brian M. Sweet, Chris B. Rogers, Daniel C. Hake, and Daniel J. Rogers. [n.d.]. Caterpillar locomotion: A new model for softbodied climbing and burrowing robots.

[35] Andreas Wächter and Lorenz T Biegler. 2006. On the implementation of an interior-point filter line-search algorithm for large-scale nonlinear programming. *Mathematical programming* 106, 1 (2006), 25–57.

[36] Feng-Yu Xu, Feng-You Jiang, Quan-Sheng Jiang, and Yu-Xuan Lu. 2020. Soft Actuator Model for a Soft Robot With Variable Stiffness by Coupling Pneumatic Structure and Jamming Mechanism. *IEEE Access* 8 (2020), 26356–26371. https://doi.org/10.1109/ACCESS.2020.2968928 Conference Name: IEEE Access.

[37] Zeyu Yan and Huaishu Peng. 2021. FabHydro: Printing Interactive Hydraulic Devices with an Affordable SLA 3D Printer. In *The 34th Annual ACM Symposium on User Interface Software and Technology* (Virtual Event, USA) *(UIST '21)*. Association for Computing Machinery, New York, NY, USA, 298–311. https://doi.org/10.1145/3472749.3474751

[38] Chen Yang, Manish Boorugu, Andrew Dopp, Jie Ren, Raymond Martin, Daehoon Han, Wonjoon Choi, and Howon Lee. 2019. 4D printing reconfigurable, deployable and mechanically tunable metamaterials. *Material Horizons* 6 (2019), 1244–1250. Issue 6. https://doi.org/10.1039/C9MH00302A

[39] Dian Yang, Bobak Mosadegh, Alar Ainla, Benjamin Lee, Fatemeh Khashai, Zhigang Suo, Katia Bertoldi, and George M. Whitesides. 2015. Buckling of Elastomeric Beams Enables Actuation of Soft Machines. *Advanced Materials* 27, 41 (2015), 6323–6327. https://doi.org/10.1002/adma.201503188 arXiv:https://onlinelibrary.wiley.com/doi/pdf/10.1002/adma.201503188

[40] Humphrey Yang, Tate Johnson, Ke Zhong, Dinesh K. Patel, Gina Olson, Carmel Majidi, Mohammad Islam, and Lining Yao. 2022. ReCompFig: Designing Dynamically Reconfigurable Kinematic Devices Using Compliant Mechanisms and Tensioning Cables. In *Proceedings of the 2022 CHI Conference on Human Factors in Computing Systems* (New Orleans, LA) *(CHI '22)*. Association for Computing Machinery, New York, NY, USA. https://doi.org/10.1145/3491102.3502065

[41] Lining Yao, Ryuma Niiyama, Jifei Ou, Sean Follmer, Clark Della Silva, and Hiroshi Ishii. 2013. PneUI: Pneumatically Actuated Soft Composite Materials for Shape Changing Interfaces. In *Proceedings of the 26th Annual ACM Symposium on User Interface Software and Technology* (St. Andrews, Scotland, United Kingdom) *(UIST '13)*. Association for Computing Machinery, New York, NY, USA, 13–22. https://doi.org/10.1145/2501988.2502037

[42] Meng Yu, Weimin Yang, Yuan Yu, Xiang Cheng, and Zhiwei Jiao. 2020. A Crawling Soft Robot Driven by Pneumatic Foldable Actuators Based on Miura-Ori. *Actuators* 9, 2 (June 2020), 26. https://doi.org/10.3390/act9020026 Number: 2 Publisher: Multidisciplinary Digital Publishing Institute.